Hindawi
International Journal of Antennas and Propagation
Volume 2019, Article ID 2126879, 9 pages
https://doi.org/10.1155/2019/2126879

Research Article

Helical Slot Antenna for the Microwave Ablation

Moonhee Lee and Taeho Son

Soonchunhyang University, Soonchunhyang-ro 22, Sinchang-myeon, Asan-si, Chungcheongnam-do, Republic of Korea

Correspondence should be addressed to Taeho Son; thson@sch.ac.kr

Received 7 June 2019; Revised 12 August 2019; Accepted 26 September 2019; Published 30 October 2019

Academic Editor: Symeon Nikolaou

In this study, a thin coaxial antenna for microwave ablation (MWA) is proposed. A helical slot is added between two slots in order to overcome the disadvantage of the radiation range extending to the unwanted part in the conventional single-slot and double-slot applicators. By adding a helical slot, the specific absorption rate (SAR) pattern is more concentrated near the slot as compared with the conventional slot. Experiments were conducted using the simulation, and a liver phantom was made and heated up using microwaves. Based on the results on the liver phantom, experiments were conducted using swine liver which is similar to human liver. Applied frequency and microwave average input power were assumed as 2.45 GHz and 50 W (47 dBm), respectively. As a result of the experiment, return loss was −23.09 dB, and the temperature reached 60°C after 90 seconds of exposition. Based on the phantom experiments of the swine liver, necrotic lesions of the tissue at a distance of 3.5–4 cm from the microwave antenna were observed.

1. Introduction

Most people have cancer cells in their bodies. These tumor cells grow on their own through ingestion of nutrients from the outside of the body (naturally without any specific major cause) or by other factors (drinking alcohol, smoking, etc.). Cancerous cells can go anywhere through the blood, and when the moved cancer cells are malignant, they can cause damage to other tissues around them [1, 2].

Methods of treating cancer cells include surgical removal through open surgery and treatment using drugs. Other treatments using electromagnetic waves such as radio frequency ablation (RFA) and microwave ablation (MWA) are well known. RFA and MWA procedures have been actively developed in recent years [3]. Generally, these methods utilized needle-shaped antennas to radiate electromagnetic waves to vibrate water molecules in the cell and heat a tumor tissue to 45°C or higher to induce the death of malignant cells. The temperature of 45°C or higher is needed for hyperthermia treatment that uses the temperatures between 41 and 45°C, which does not completely kill the tumor cells through changing the resistance of the cell and inhibiting their activity. However, when temperatures that are higher than 45°C are delivered to cells, protein structure and DNA are completely destroyed. This is the reason why MWA procedure referred to as thermal ablation is commonly used in medical practice [4–6].

The antenna used in the MWA method employs an air slot inside the coaxial cable to allow microwave (MW) radiation and tissue heating. Various methods including changing the number of slots, adding chokes, combining with monopole antennas, and many others are being studied within needle microwave applicators. If the number of slots is reduced, the radiation range widens and power transmitted the tissue is relatively reduced. As a result, the healthy cells outside the tumor could be damaged. In addition, the liver tissue phantom was not frequently used in the MWA experiment, and the results regarding the microwave radiation time were not clear. The operating range can be controlled by the input power delivered to the antenna. Additionally, when the double-slot antenna is applied, the MW radiation range is concentrated compared with the single-slot applicator, but when the input power increased, the range to be transmitted becomes higher again [7–17].

Therefore, in this study, the needle-type coaxial antenna with a helical slot was proposed to prevent distribution of the

MW radiation range for several existing methods using single-slot and double-slot antennas and to reduce EM wave exposure. The application of the helical slot has the advantage of concentrating the range near the slot even when the input power is increased. The applied antenna operating frequency of 2.45 GHz is from the Industrial Scientific Medical (ISM) band and the input power is 50 W, as well as the liver tissue is calibrated to the human tissue in terms of electrical and thermal properties. For simulation, ANSYS HFSS commercial simulation software and COMSOLTM MULTIPHYSICS were used. The HFSS and MULTIPHYSICS are commercial software based on the finite element method (FEM). The simulation uses a liver phantom similar in electrical characteristics to human liver tissue. What is more, the experiment was conducted using a swine liver which is similar to a human liver.

2. Methods and Model

2.1. Physical Principles. The physical principle of MWA is that the application of an electromagnetic field (EMF) on biological tissue produces an effect called dielectric relaxation. This phenomenon in which polar molecules, like water, try to continuously rearrange in the external EMF, which has polarity changing several billions of times per second. Since the molecules cannot keep up with the change in the EMF, excessive energy is applied to the tissue as heat. However, the amount of heat is not the determinant value for assessing the amount of power being absorbed by the tissue. Therefore, one of the methods of analyzing the thermal effect of the MWA antenna is to measure the specific absorption rate (SAR). The SAR parameter represents the amount of EM power dissipated in a unit mass of tissue (W/kg) in any position vector location and its mathematical expression is as follows:

$$\mathrm{SAR} = \frac{\sigma}{2\rho}|\mathbf{E}|^2, \tag{1}$$

where σ represents the tissue conductivity (S/m), ρ is the tissue density (kg/m^3), and $|\overline{E}|$ is the magnitude of the electrical field strength (V/m). In general, it is desirable to prevent the formation of a backward heating pattern in which the SAR is greater for the region focused at the distal tip of the antenna and the temperature of the rest of the antenna rises. Therefore, the electrical efficiency of interstitial antennas depends on their geometry and insertion depth [18].

The Pennes bio-heat equation effectively describes how heat transfer occurs in biological tissue [19]:

$$\rho C\frac{\partial T}{\partial t} + \nabla\cdot(-k\nabla T) = \rho_{\mathrm{b}}C_{\mathrm{b}}\omega_{\mathrm{b}}\left(T_{\mathrm{b}} - T\right) + Q_{\mathrm{met}} + Q_{\mathrm{ext}}, \tag{2}$$

where k is the thermal conductivity of the tissue (W/m∗k), ρ_{b} is the blood density (kg/m^3), C_{b} is the blood specific heat (J/kg∗k), and ω_{b} is the blood perfusion rate (1/s). T_{b} is the body temperature (°C), T is the final temperature (°C), Q_{met} is the heat source from metabolism (W/m^3), and Q_{ext} represents an external heat source (W/m^3). Another important element of MWA is the effective wavelength of the antenna. It determines the magnitude of the wavelength that propagates through the tissue. The geometry of the antenna is determined through the effective wavelength defined as

$$\lambda_{\mathrm{eff}} = \frac{c}{f\sqrt{\varepsilon_{r'}}}, \tag{3}$$

where $\varepsilon_{r'}$ represents the real part of complex relative permittivity of the tissue, c is the speed of light in free space (m/s), and f is the frequency (Hz) of the source signal [20–22].

Table 1: Properties of liver tissue.

Parameters	Values
Relative permittivity	43.035
Electric conductivity	1.6864 S/m
Loss tangent	0.27851
Density of liver tissue	1079 kg/m^3
Specific heat capacity of blood	3540 J/kg∗°C
Thermal conductivity	0.52 W/m∗°C
Metabolic heat source	33,800 W/m^3

2.2. Liver Phantom. The liver phantom was used before the experiment with swine liver. The electrical characteristics of the liver phantom are similar to those of the human liver. The phantom mainly consists of distilled water, sucrose, sodium chloride, hydroxyethyl cellulose (HEC) 440 (kind of glycerin), and Dowicil (kind of antiseptic). The dielectric characteristics of the real human liver are as follows [20]: an electrical conductivity of 1.6864 S/m, a relative permittivity of 43.035, and a loss tangent of 0.27851. The liver phantom was produced based on these measured parameters of the liver. To demonstrate the similarity of real hepatic tissue, the liver phantom's electric characteristics were measured using the Agilent's dielectric characteristic measuring device (85070E). The liver phantom is made of distilled water 48.8%, sucrose 47.56%, sodium chloride 1.21%, and Tween 20 (kind of surface active agent) 2.43%. The liver phantom's electrical conductivity was assumed as 1.7434 S/m, relative permittivity was assumed as 43.8213, and loss tangent was assumed as 0.2919 [23, 24].

Another important consideration was the thermal characteristics of the human liver defined by the following parameters: density 1079 kg/m^3, thermal conductivity 0.52 W/m∗°C, specific heat 3540 J/kg∗°C, and metabolic heat source 33,800 W/m^3. The simulation of the liver tissue phantom was produced based on these thermal parameters (Table 1).

2.3. Helical Slot Antenna. Figure 1(a) shows a schematic view of internal construction of the coaxial antenna with a helical slot. The coaxial antenna consists of a central conductor $r_1 = 0.25$ mm, dielectric $r_2 = 0.82$ mm, outer conductor $r_3 = 1.09$ mm, and catheter $r_4 = 1.5$ mm. The central conductor and the outer conductor are made of copper, dielectric, and catheter's material is polytetrafluoroethylene (PTFE). Figure 1(b) shows the slot part of analyzed coaxial

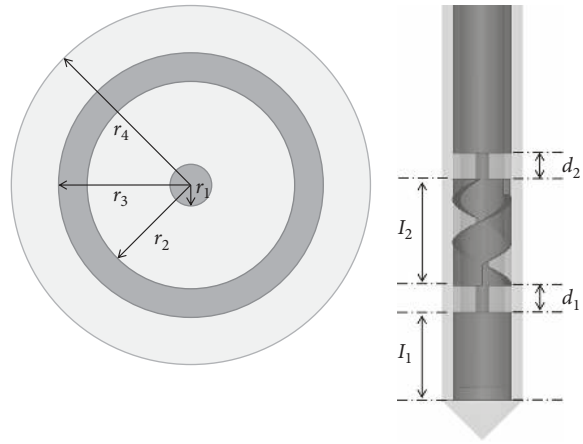

Figure 1: (a) Schematic view of internal construction of the coaxial antenna and (b) helical slot part.

antenna. A helical slot was placed between double slots, with a total height l_2 of 3 mm; helical slot's height was 1.2 mm and the slot turned 1.3 turns. The height of the two slots were placed horizontally where $d_1 = d_2 = 1$ mm , and the distance between the first slot and the end of the coaxial antenna was $l_1 = 4$ mm (Table 2).

The proposed model includes the following assumptions, namely, the hepatic tissue is considered as linear, homogenous, and isotropic medium, and the wave equation under time harmonic conditions is expressed as [24]

$$\nabla \times \left[(\varepsilon_r)^{-1} \nabla \times \mathbf{H} \right] - \mu \omega^2 \mathbf{H} = 0. \tag{4}$$

In the aforementioned equation, **H** stands for a complex-valued vector of magnetic field intensity (A/m). $\omega = 2\pi f$ is the angular frequency of EM field source (rad/s), and μ is a permeability of tissue (H/m). What is more, the frequency-dependent complex permittivity with its real and imaginary parts is presented as

$$\varepsilon(\omega) = \varepsilon_0 \varepsilon_r = \varepsilon_0 \left(\varepsilon_{r'} - j \frac{\sigma}{\omega \varepsilon_0} \right), \tag{5}$$

where$\varepsilon_0 = 8.85 \times 10^{-12}$ F/m is the electric constant and σ is an electrical conductivity of liver tissue. Due to axis symmetry, the transverse magnetic (TM) waves are utilized with magnetic and electric field components as follows: $\mathbf{H} = H_\phi \mathbf{e}_\phi$ and $\mathbf{E} = E_r \mathbf{e}_r + E_z \mathbf{e}_z$. The magnetic field **H** has a tangential component. The electric field **E** propagates in the r–z plane. What is more, the magnetic field at the feeding port is established by the total input power P_{in} (W) of the microwave antenna using the so-called port boundary condition at the antenna feeding [25]:

$$H_{\varnothing 0} = \frac{1}{z_r} \sqrt{\frac{Z P_{\text{in}}}{\pi \ln(r_2/r_1)}}, \tag{6}$$

where r_1 and r_2 represent the inner and outer radii of the dielectric coaxial cable, respectively, and $Z = 120\pi/\sqrt{\varepsilon_{r'}}$ (Ω) is the dielectric wave impedance. In the next step, the electric field intensity **E** (V/m) is calculated from Faraday's law.

Table 2: Properties of antenna.

Parameters	Values
Electric conductivity of dielectric	0 S/m
Relative permeability of dielectric	1
Relative permittivity of catheter	2.03
Electric conductivity of catheter	0 S/m
Relative permeability of catheter	1
Relative permittivity of conductor	1
Electric conductivity of conductor	0 S/m
Relative permeability of conductor	1

Figures 2(a) and 2(b) show simulation of a coaxial antenna and the liver phantom. The total length of the antenna was 95 mm, and the used liver phantom's size was (a) 50 mm × (b) 30 mm × (c) 50 mm. The insert depth was 24 mm.

3. Measurement and Obtained Results

Figure 3 shows the result of the return loss of simulation and measurement using a network analyzer of the coaxial antenna at 2.45 GHz inside the liver phantom. Return loss obtained was −23.0878 dB in simulation and −21.0472 dB in the actual phantom. The results of simulation and measurement of actual phantom were satisfied at 2.45 GHz.

The different resonance frequencies between the simulation and the measurement come from the different dielectric constants between them, and also the measurement environment is not same as the simulations. The return loss result can be controlled by inserted depth of the coaxial antenna. Therefore, in real human liver experiment, researchers can modulate the length of the antenna depending on the location of the cancer. If the tumor is deeply located, the insertion depth can be adjusted to the total length of the antenna except for the antenna slot part.

Figure 4 shows the radiation pattern of the coaxial antenna with helical slots. In the case of the inner and outer conductors being grounded, the slot is taken out in the horizontal and diagonal directions to induce the radiation so that the radiation is formed in a slight 8-shaped pattern.

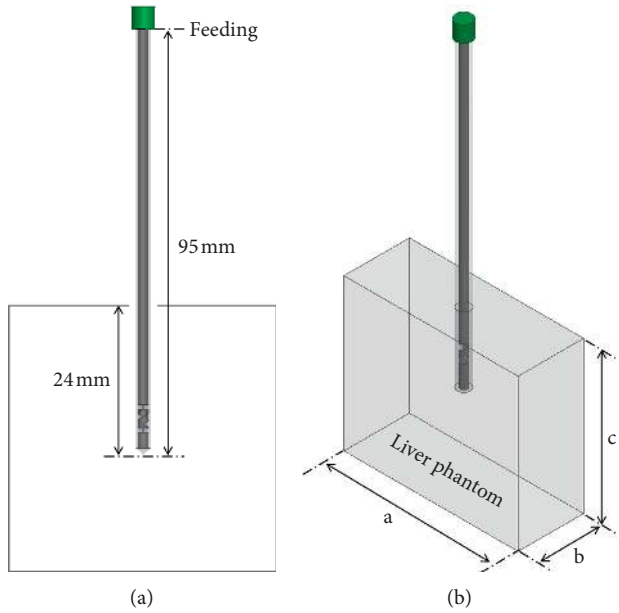

Figure 2: (a) Total view of the inserted antenna and dimensions of length and depth. (b) The view of the inserted antenna into the liver phantom.

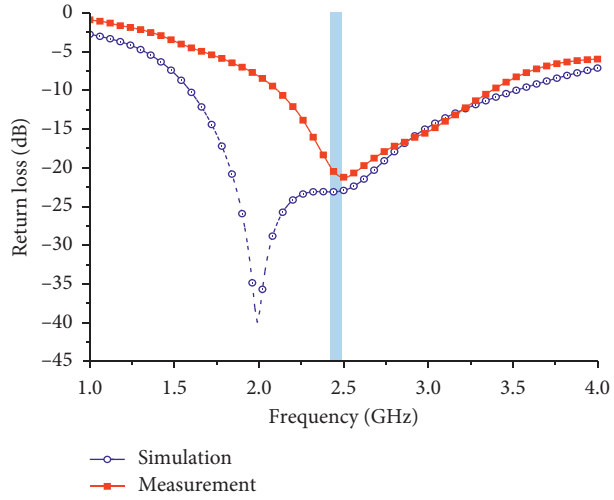

Figure 3: Return loss of measurement and simulation in liver phantom.

The SAR distribution in Figure 5 shows a similar pattern. It was obtained with the ANSYS HFSS tool. The overall shape has an elliptical radiation pattern around the slot, and the instantaneous range that directly affects the liver tissue is about 2 to 3 cm.

Figure 6 shows the temperature changes in the liver phantom over time with the application of the 50 W microwave input power based on the radiation pattern using a thermal imaging camera. The thermal imaging camera measurement is focused on the helical slot part. Microwave was radiated based on the fact that the protein structure and DNA of liver tissue can be perfectly destroyed when the heat temperature applied goes above 45°C and up to 60°C. As a result, the liver tissue's temperature reached around 60°C in about 90 to 120 seconds, while the microwave operating starts at a normal human body temperature of 37°C. The treatment time is dependent on the size of the tissue. However, the immediate vicinity of the helical slot antenna is heated the most effectively. Figure 7 shows the temperature changes over time of the liver phantom for antenna without the helical slot part. It turned out that it takes much longer to reach the same temperature level around 60°C. As a result, the antenna with the helical slot is more efficient.

Figure 8 shows comparison of temperature over time for both antenna types. The time necessary to reach 60 degrees of Celsius for the antenna with the helical slot is approximately 90 seconds, and the time to reach the same temperature level for the antenna without the helical slot is about

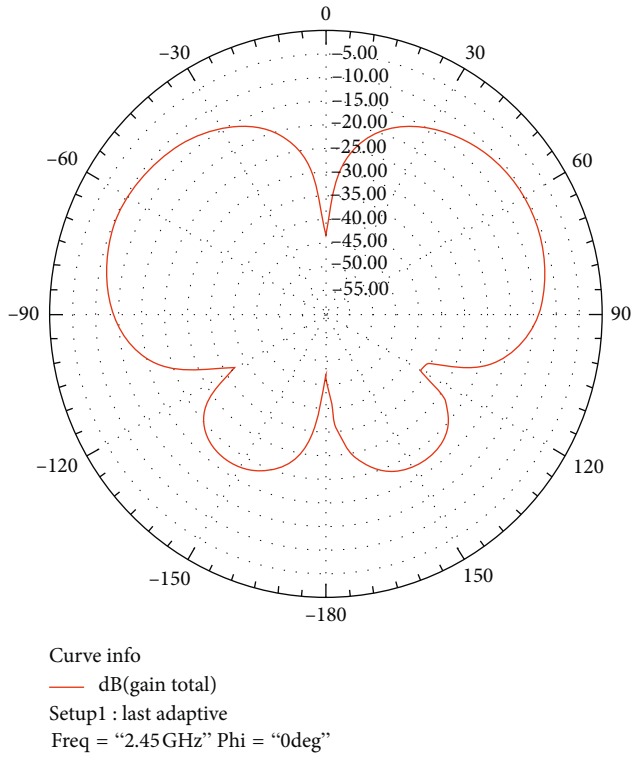

Figure 4: Radiation pattern of the coaxial antenna (with helical slots).

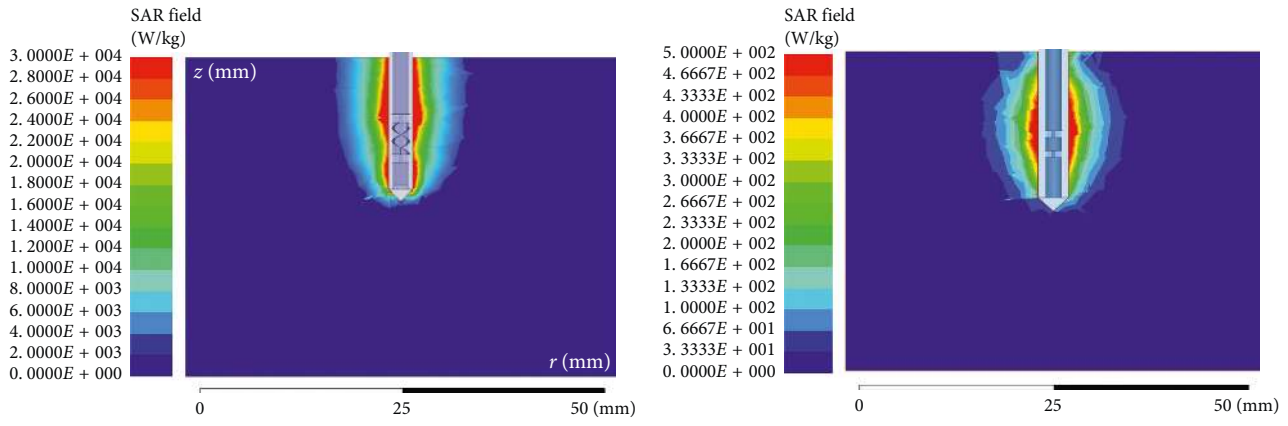

Figure 5: The result of the SAR pattern for the steady state: (a) antenna with the helical slot part and (b) antenna without the helical slot part.

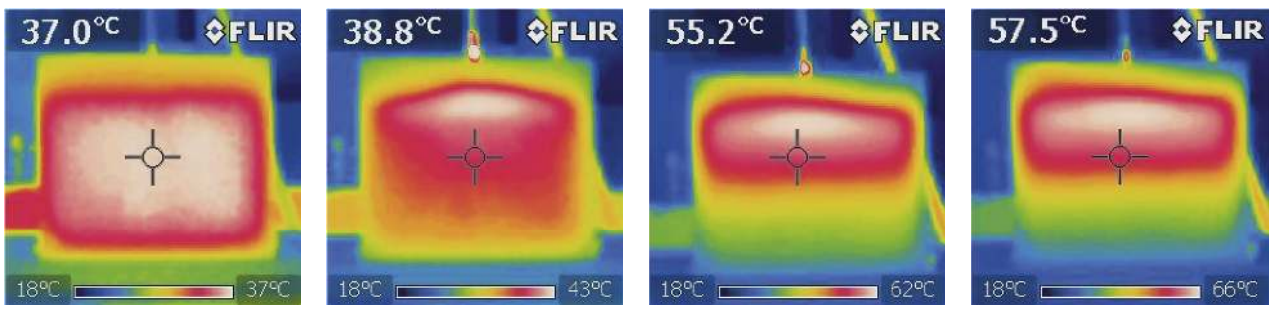

(a) (b) (c) (d)

Figure 6: Temperature changes over time on the liver phantom: (a) start, (b) 30 sec, (c) 60 sec, and (d) 90 sec in the case of antenna with the helical slot.

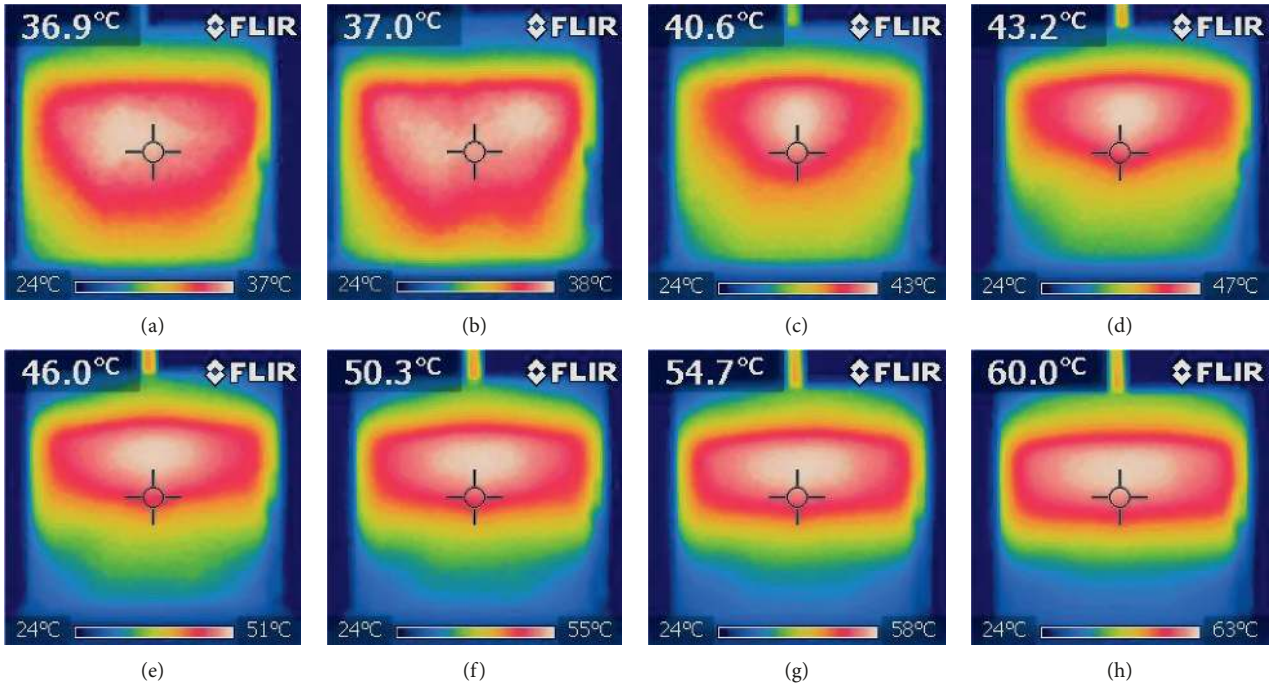

Figure 7: Temperature changes over time on the liver phantom: (a) start, (b) 30 sec, (c) 60 sec, (d) 90 sec, (e) 120 sec, (f) 150 sec, (g) 180 sec, and (h) 210 sec in the case of antenna without the helical slot.

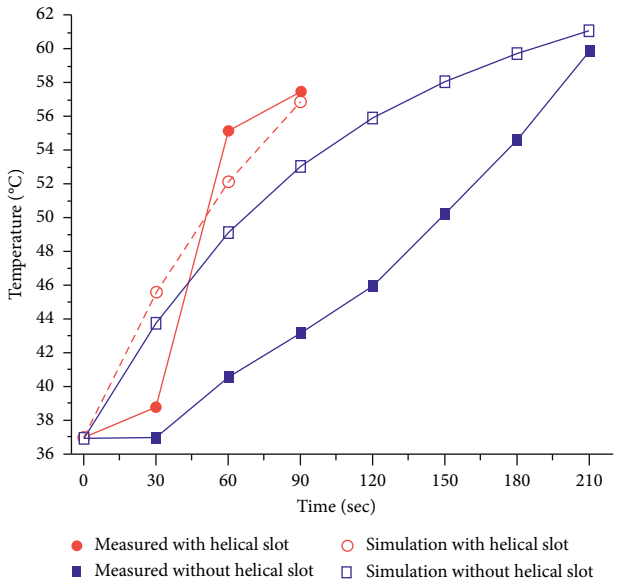

Figure 8: Comparison of temperature distributions over time in the case of antennas with helical slot and without it.

210 sec. Simulation results are similar to measured results. The MWA process can be calculated as a finite element model (FEM) coupled equations of electromagnetic field and the bio-heat transfer equation via COMSOLTM MULTI-PHYSICS. The transferred heat is generated externally by the electromagnetic field by the Pennes biothermal equation.

Figure 9 shows the temperature changes over time of the real swine liver using the same thermal imaging camera as used in Figures 6 and 7. The result of tissue heating presented in Figure 9 is shown in Figure 10(a). In Figure 6, it took 90 seconds to reach 60°C when the antenna with the helical slot was measured on the tissue phantom. On the basis of this measurement, the temperature changes were measured in the real swine liver up to 90 seconds every 30 seconds. The temperature changes are similar with the experiment on the liver phantom as presented in Figure 6.

Figure 11(a) and Figure 11(b) show views of whole implemented antenna and its helical slot part.

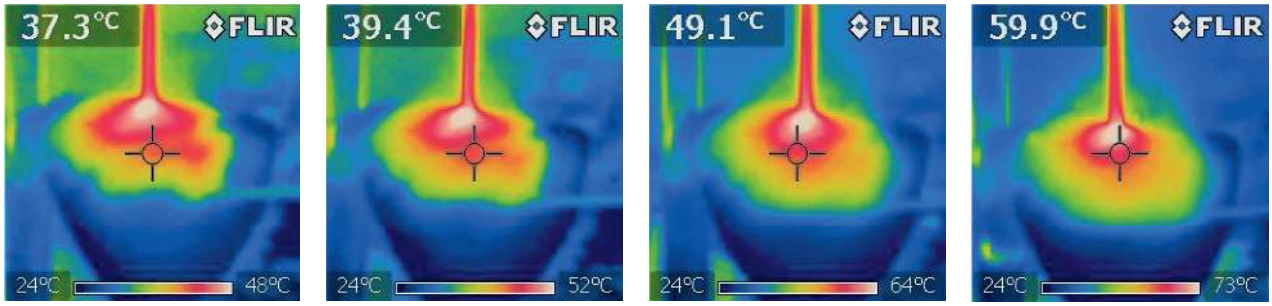

(a) (b) (c) (d)

Figure 9: Temperature changes over time on the swine liver: (a) start, (b) 30 sec, (c) 60 sec, and (d) 90 sec.

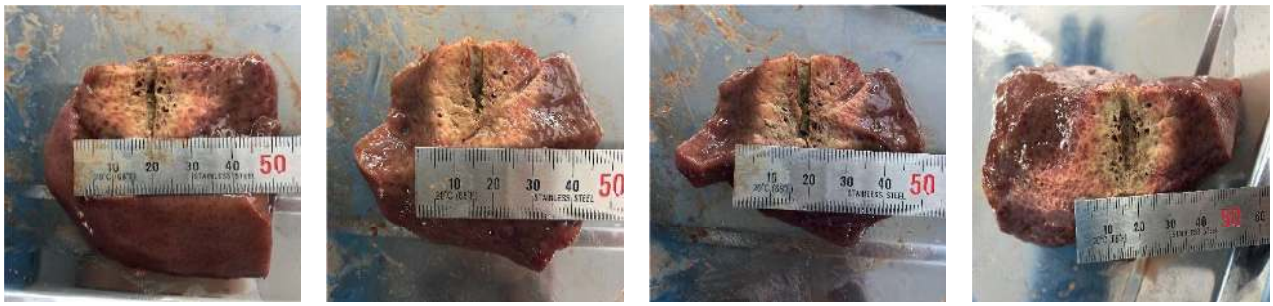

(a) (b) (c) (d)

Figure 10: Experiment on the 4 different swine livers.

(a) (b)

Figure 11: Views of (a) implemented antenna and (b) helical slot part.

Figure 10 shows the real experiment on the 4 different swine livers. The swine liver is biologically similar to the human liver and is widely used as a test object in animal studies at the stage immediately before the clinical trial of medical studies [26, 27]. The coaxial antenna inserted in the liver tissue caused the microwave heating. The change of tissue temperature was confirmed through the real-time thermal imaging camera. The size of the swine liver was based on the phantom experiment. The minimum size of phantom was 50 mm × 30 mm × 50 mm, and the insertion

depth of the coaxial antenna was 24 mm. As demonstrated in Figure 10, the microwave heating resulted in the coagulation of liver tissue in the distance 3.5–4 cm from the used antenna. The shape of the coagulated tissue is similar with the radiation pattern and the SAR pattern like a sphere.

4. Conclusion

In this study, a helical slot antenna for tumor microwave heating was proposed. To overcome the disadvantages of single-slot and double-slot needle applicators and to control the radiation range, a helical slot was added between two horizontal slots. The ANSYS HFSS commercial software was used for simulation. Importantly, the authors made a liver phantom that had dielectric parameters similar to those of the human liver. Afterwards, through the simulation using the phantom experiment, the proper time data for the real ex vivo experiment were achieved. As a result, part of liver tissue was coagulated in a distance of 3.5–4 cm from used antenna.

It is worth noted that more studies are needed to verify the radiation and temperature distribution based on the number of antennas at close distances and clinical trials through real human liver instead of swine liver.

Data Availability

The simulation and measurement data used to support the findings of this study are available from the corresponding author upon request.

Conflicts of Interest

The authors declare that there are no conflicts of interest regarding the publication of this paper.

Acknowledgments

This research was supported by the Basic Science Research Program through the National Research Foundation of Korea (NRF) funded by the Ministry of Education (2015023260) and by the Soonchunhyang University Research Fund.

References

[1] B. R. Lane, J. Bissonnette, T. Waldherr et al., "Development of a center for personalized cancer care at a regional cancer center," *The Journal of Molecular Diagnostics*, vol. 17, no. 6, pp. 695–704, 2015.

[2] A. Razib, K. A. Hossain, and S. Hossain, "Microwave ablation technique (MWA) for cancer treatment," in *Proceedings of the 2016 International Conference on Medical Engineering, Health Informatics and Technology (MediTec)*, pp. 1–6, Dhaka, Bangladesh, December 2016.

[3] P. Cala and P. Bienkowski, "The concept and design of an interstitial microwave hyperthermia antenna with directional radiation characteristics," *Przeglad Elektrotechniczny*, vol. 94, no. 1, pp. 9–12, 2018, In polish.

[4] P. Gas, "Optimization of multi-slot coaxial antennas for microwave thermotherapy based on the S_{11}-parameter analysis," *Biocybernetics and Biomedical Engineering*, vol. 37, no. 1, pp. 78–93, 2017.

[5] R. J. L. Roti, "Cellular responses to hyperthermia (40–46°C): cell killing and molecular events," *International Journal of Hypeerthermia*, vol. 24, no. 1, pp. 3–15, 2008.

[6] S. P. Singh, "Microwave applicators for hyperthermia treatment of cancer an overview," in *Proceedings of the 2018 3rd International Conference on Microwave and Photonics (ICMAP)*, pp. 1–3, Dhanbad, India, February 2018.

[7] Y. Wang, Y. Sun, L. Feng, Y. Gao, X. Ni, and P. Liang, "Internally cooled antenna for microwave ablation: results in ex vivo and in vivo porcine livers," *European Journal of Radiology*, vol. 67, no. 2, pp. 357–361, 2008.

[8] M. D. Sawarbandhe, B. S. Naik, V. R. Satpute, and S. Saugata, "Coaxial antenna for microwave ablation," in *Proceedings of the 2016 IEEE Distributed Computing, VLSI, Electrical Circuits and Robotics (DISCOVER)*, pp. 119–122, Mangalore, India, August 2016.

[9] N. Tal and Y. Leviatan, "A minimally invasive microwave ablation antenna," in *Proceedings of the 2017 IEEE International Conference on Microwaves, Antennas, Communications and Electronic System (COMCAS)*, pp. 1–3, Tel-Aviv, Israel, November 2017.

[10] K. Ito, K. Saito, T. Taniguchi, S. Okabe, and H. Yoshimura, "Minimally invasive thermal therapy for cancer treatment by using thin coaxial antennas," in *Proceedings of the 23rd Annual International Conference of the IEEE Engineering in Medicine and Biology Society*, vol. 4, pp. 3314–3317, Istanbul, Turkey, Turkey, October 2001.

[11] C. F. Huang, C. F. Li, and H. Y. Chao, "The study of SAR distribution in microwave ablation for tumours," in *Proceedings of the 2015 Asia-Pacific Symposium on Electromagnetic Compatibility (APEMC)*, pp. 24–26, Taipei, Taiwan, May 2015.

[12] R. Ortega-Palacios, A. Vera, and L. Leija, "Microwave ablation coaxial antenna computational model slot antenna comparison," in *Proceedings of the 2012 Pan American Health Care Exchanges (PAHCE)*, pp. 58–61, Miami, FL, USA, March 2012.

[13] H. Fallahi and P. Prakash, "Antenna designs for microwave tissue ablation," *Critical Reviews in Biomedical Engineering*, vol. 46, no. 6, pp. 495–521, 2018.

[14] Y. Mohtashami, H. Luyen, J. F. Sawicki, J. D. Shea, N. Behdad, and S. C. Hagness, "Tools for attacking tumors: performance comparison of triaxial, choke dipole, and balun–free base–fed monopole antennas for microwave ablation," *IEEE Antennas and Propagation Magazine*, vol. 60, no. 6, pp. 52–57, 2018.

[15] C. H. nee Reimann, B. Bazrafshan, M. Schubler et al., "A dual-mode coaxial slot applicator for microwave ablation treatment," *IEEE Transactions on Microwave Theory and Techniques*, vol. 67, no. 3, pp. 1255–1264, 2019.

[16] P. Gas, "Study on interstitial microwave hyperthermia with multi-slot coaxial antenna," *Revue Roumaine des Sciences Techniques-Serie Electrotechnique et Energetique*, vol. 59, no. 2, pp. 215–224, 2014.

[17] Y. Xu, M. A. J. Moser, E. Zhang, Z. Wenjun, and Z. Bing, "Large and round ablation zones with microwave ablation: a Preliminary study of an optimal aperiodic tri-slot coaxial antenna with the π–matching network section," *International Journal of Thermal Sciences*, vol. 140, pp. 539–548, 2019.

[18] P. Gas and A. Miaskowski, "SAR optimization for multi-dipole antenna array with regard to local hyperthermia," *Przeglad Elektrotechniczny*, vol. 95, no. 1, pp. 17–20, 2019.

[19] P. Gas and B. Szymanik, "Shape optimization of the multi-slot coaxial antenna for local hepatic heating during microwave

ablation," in *Proceedings of the 2018 International Interdisciplinary PhD Workshop (IIPhDW)*, pp. 319–322, Swinoujście, Poland, May 2018.

[20] J. E. Lara, A. Vera, L. Leija, and M. I. Gutiérrez, "Modeling of electromagnetic and temperature distributions of an interstitial coaxial-based choked antenna for hepatic tumor microwave ablation," in *Proceedings of the 2015 12th International Conference on Electrical Engineering, Computing Science and Automatic Control (CCE)*, pp. 1–5, Mexico City, Mexico, October 2015.

[21] K. L. Clibbon and A. McCowen, "Efficient computation of SAR distributions from intersticial microwave antenna arrays," *IEEE Transactions on Microwave Theory and Techniques*, vol. 42, no. 4, pp. 595–600, 1994.

[22] W. Jakawanchaisri, A. Sanpanich, P. Phasukkit et al., "FEM analysis of microwave ablation for snoring therapy," in *Proceedings of the 2012 2nd Internaional Conference in Biomedical Engineering and Technology (IPCBEE)*, vol. 34, pp. 22–26, Singapore, 2012.

[23] P. Keangin, P. Rattanadecho, and T. Wessapan, "An analysis of heat transfer in liver tissue during microwave ablation using single and double slot antenna," *International Communications in Heat and Mass Transfer*, vol. 38, no. 6, pp. 757–766, 2011.

[24] P. Prakash, M. C. Converse, D. M. Mahvi, and G. W. John, "Measurement of the specific heat capacity of liver phantom," *Physiological Measurement*, vol. 27, no. 10, pp. N41–N46, 2006.

[25] P. Gas, "Multi frequency analysis for interstitial microwave hyperthermia using multi slot coaxial antenna," *Journal of Electrical Engineering*, vol. 66, no. 1, pp. 26–33, 2015.

[26] A. Nykonenko, P. Vávra, and P. Zonča, "Anatomic peculiarities of pig and human liver," *Experimental and Clinical Transplantation*, vol. 15, no. 1, pp. 21–26, 2017.

[27] C. F. Huang, Y. W. Tien, C. Y. Chen, and L. Xi-Zhang, "Design techniques for antenna needles used in microwave hyperthermia therapy for tumor treatment," in *Proceedings of the 2014 IEEE-APS Topical Conference on Antennas and Propagation in Wireless Communications (APWC)*, pp. 37–39, Palm Beach, Netherlands Antilles, August 2014.